Interfacial templating of inorganic nanostructures using a growth directing and reducing peptide

ARTICLE *in* SOFT MATTER · OCTOBER 2011

Impact Factor: 4.03 · DOI: 10.1039/C1SM05906H

4 AUTHORS, INCLUDING:

Lorraine Leon
University of Chicago
21 PUBLICATIONS **55** CITATIONS
SEE PROFILE

Hiroshi Matsui
City University of New York - Hunter College
102 PUBLICATIONS **3,002** CITATIONS
SEE PROFILE

Raymond Tu
City College of New York
20 PUBLICATIONS **297** CITATIONS
SEE PROFILE

Soft Matter

Cite this: DOI: 10.1039/c1sm05906h

www.rsc.org/softmatter

PAPER

Interfacial templating of inorganic nanostructures using a growth directing and reducing peptide†

Lorraine Leon,[a] Wei Su,[b] Hiroshi Matsui[b] and Raymond Tu*[a]

Received 16th May 2011, Accepted 15th August 2011
DOI: 10.1039/c1sm05906h

The rational design of interfacially confined peptides allows for the direct examination of biomimetic processes for materials synthesis, where non-equilibrium interfacial assembly engenders complexity in metallic nano-structures. Here we report our recent progress towards applying surface-active peptides to precisely control the spatial distribution of amino acids. In order to engineer multiple length scales in inorganic materials, our periodically sequenced peptide is designed to be trifunctional: (1) self-assembling at the air–water interface, (2) reducing gold in the subphase, and (3) directing growth of the inorganic phase under confinement. We use the Langmuir trough, Brewster angle microscopy, atomic force microscopy, transmission electron microscopy and electron diffraction to characterize control over inorganic structure as a function of the surface pressure of the organic material at the interface. Single crystalline triangular nanoplatelets of gold form at a surface pressure of 30 mN m^{-1} or less. At higher surface pressures, when binding sites are in closer proximity, a mosaic of more complex structures are formed. This work demonstrates that self-assembling surface confined peptides can be applied to define a bio-inspired tectonic process, leading to hierarchical structures at phase boundaries.

Introduction

Biological organisms organize inorganic materials into complex nanostructures by coupling self-assembly of the organic phase with the ability to direct growth of the inorganic phase.[1–4] This mechanism has inspired engineers to develop hybrid materials at the nanometre scale, where the properties of metals and semiconductors show unique electronic, optic, and catalytic properties.[5,6] Several methodologies have been developed to engineer functional nanoscale materials. Although, in order to precisely engineer materials with hierarchical length scales, top-down approaches are typically applied, which are limited by cost or availability of short wavelength lasers. An alternative is using bottom-up techniques to arrange atoms into nanostructures, which is limited by the complexity of structures accessible. Our work is inspired by biological composite materials where both nanoscale features and complexity are realized through non-equilibrium assembly processes.[7]

Many bottom-up techniques form gold nanoparticles. Early methodologies apply citrate reductants to form simple spherical gold nanoparticles,[8] but anisotropic nanoparticles such as nanorods,[9,10] nanocubes,[11] triangular platelets,[12] and nanostars[13] have also been observed using seed mediated approaches that employ strong reductants to produce the initial seed, increasing issues with toxicity and expense, therefore the use of biomimetic systems circumventing these issues may be an efficient pathway.[14,15] In contrast, biomimetic templating agents have guided the assembly of particles into more complex structures such as nanochains[16] and double helices.[17]

Several peptide-based approaches exist to template inorganic materials.[18–21] In the case of gold, histidine-rich peptides have been applied to decorate the shell of nanotubes,[22] templating a shell of isotropic gold nanoparticles along the perimeter. Also, reports exist of β-sheet forming peptides that self-assemble into fibres producing laterally spaced linear nanoparticle arrays based on the location of charged residues within the fibril.[23,24] However, in each case inorganic nanoparticles are formed using reducing agents prior to exposure to the organic template. Recently, tryptophan has been used as a non-toxic method to synthesize spherical nanoparticles at room temperatures and anisotropic particles at higher temperatures.[25] Also, Slocik *et al.* report a one pot synthesis of spherical particles using a peptide with biomolecular recognition properties[26] and Brown *et al.* use polypeptide sequences identified using phage display to synthesize triangular platelets.[27] Similarly, gold nanoparticles of multiple sizes and shapes have been synthesized *in situ* using peptide amphiphile hydrogels[28] and lemongrass extract has been used to generate triangular platelets.[29]

The surface plasmon resonance behaviour in gold nanostructures has been applied to develop sensors of sizes comparable to single biological molecules, which could further the understanding of complex biological systems.[30–32] In particular,

[a]*Department of Chemical Engineering, The City College of The City University of New York, New York, USA. E-mail: tu@ccny.cuny.edu*
[b]*Department of Chemistry, Hunter College of The City University of New York, New York, USA*

† Electronic supplementary information (ESI) available. See DOI: 10.1039/c1sm05906h

triangular nanoplatelets are attractive candidates for sensing and surface enhanced Raman spectroscopy because the sharp edges lead to high local electric field gradients under illumination.[10] This effect is even more prevalent in structures such as a star that displays more than three sharp edges.[13] In addition, outside of sensing, particles of this nature have applications in catalysis,[8,33] conductive tips in scanning tunnel microscopy,[29] and the hyperthermic treatment of cancerous tumors.[34,35]

We report a peptide molecule that self-assembles at the air–water interface and is capable of reducing gold ions and coordinating them to form triangular nanoplatelets and related structures. We show that we are able to control both morphology and crystallinity as a function of surface pressure. Other two-dimensional techniques that template gold at different surface pressures involve polymers,[36] lipids,[37] and diacetylene[38] molecules, each requiring the formation of the nanoparticles prior to the self-assembly of the organic molecules. Therefore, our system explores a template that is capable of reducing and coordinating gold-ions from the subphase to explore the template behaviour out of equilibrium, yielding varying shapes and controlled crystallinity by simply varying surface pressure without using high temperatures, reducing agents, or pre-assembled templates.

Experimental

Peptide molecules are designed in our lab and synthesized by AnaSpec (San Jose, CA) with a purity of >80%. The peptides are stored at −20 °C. Trifluoroacetic Acid, Chloroform, hexadecane, and carbon tetrachloride are obtained from Fisher Scientific (Pittsburgh, PA) and water is purified using a Millipore apparatus (Billerica, MA). Monolayers of the peptides are prepared by spreading a fresh solution of the peptide in trifluoroacetic acid/chloroform (1 : 9 v/v) at a concentration of 1mg mL^{-1} on a subphase of deionized water. Hydrogen tetrachloroaurate(III) is obtained from Sigma-Aldrich (Saint Louis, MO). Stock solution of hydrogen tetrachloroaurate(III) is freshly prepared at a concentration of 0.04 M and stored covered in foil at 4 °C. Octadecyltrichlorosilane is obtained from Acros Organics (Thermo Fisher Scientific, Waltham, MA).

Langmuir trough

Surface pressure-area isotherms are obtained using a KSV minimicro trough (KSV instruments, Helsinki, Finland). The peptides are deposited on a subphase of deionized water and are all compressed at the same speed of 5mm/min.

Brewster angle microscopy

Brewster angle microscopy images are obtained simultaneously with the surface pressure-area isotherms using an I-Elli 2000 ellipsometer/Brewster angle microscope (Nanofilm, Halcyonics, Gottingen, Germany). The resolution of the I-Elli 2000 is 1 μm in all images shown. Images are obtained before and after crystallization experiments.

Crystallization experiments

Monolayers of the peptide molecules are compressed to a given surface pressure and then 80 μL of the 0.04 M hydrogen tetrachloroaurate(III) stock solution is added to the 50 mL deionized water subphase using the injection port below the air/water interface. The ions are allowed to incubate for 10 h before samples are taken using a Langmuir–Schaefer deposition technique using carbon coated 200 mesh copper grids from Electron Microscopy Sciences (Hatfield, PA).

Transmission electron microscopy and electron diffraction

Samples are transferred from the air–water interface using a Langmuir–Schaefer technique onto carbon-coated copper Transmission Electron Microscopy (TEM) grids. Excess solution is removed by filter paper. These samples are then studied by TEM and electron diffraction (JOEL JEM-2100 Transmission Electron Microscope) at an acceleration voltage of 200 kV.

Atomic force microscopy

Samples for the atomic force microscope are obtained by transferring the peptide/gold monolayer using a Langmuir–Schaefer deposition technique using a silicon substrate that was previously coated with octadecyltrichlorosilane. The hydrophobic modification of the silicon substrate is achieved by using a procedure outlined previously by Kumar *et al.*[39] The presence of a hydrophobic layer is confirmed by measuring the contact angle, which is greater than 90°. Atomic force microscopy images are obtained using a Nanscope III instrument (Digital Instruments, Santa Barbara, CA) in tapping mode using Nanoprobe SPM (Santa Barbara, CA) tips with a resonance frequency range of 307–374 kHz and a length of 125 μm.

Results and discussion

Langmuir Blodgett techniques are used to accurately characterize the self-assembly of the peptide, Beta 9H, at the air–water interface. The peptide molecule, shown in Fig. 1, is rationally designed to form a β-sheet at the air–water interface. This design is accomplished by choosing amino acids with a high propensity to form a β-sheet[40] configuration, and the periodic sequence also defines an amphiphilic architecture, allowing us to confine the peptides to the air–water interface.[41] In addition to using an alternating hydrophobic and hydrophilic sequence of amino acids to achieve the periodicity associated with a β-sheet secondary structure, two other amino acids tryptophan and histidine are incorporated in this sequence. Tryptophan is

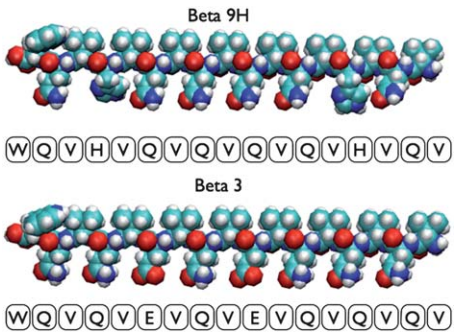

Fig. 1 The peptide molecules Beta 9H and Beta 3 rendered using van der Waals representation.

included to reduce gold ions through the transfer of electrons from the amine group of Trp to the Au^{3+} ion.[25] Histidine is included in the sequence because of its ability to form complexes with metal ions using the imidazole and amine group of sequenced peptides.[22,42,43] To verify the role that histidine plays in the process of forming gold nanoparticles, we also use a peptide called Beta 3 that does not contain histidine, but still contains the tryptophan residue. The sequence and structure of the Beta 3 molecule is also shown in Fig. 1. The self-assembly of both these molecules under two dimensional confinement has been described previously using thermodynamic models for the surface pressure-area isotherms and phase behaviour.[44] In that paper, we describe how both Beta 9H and Beta 3 are surface active and exhibit similar phase behaviour. The isotherms and Brewster angle microscopy images of the phase behaviour of Beta 9H are shown in Fig. 2. The molecules first self-assemble to form small circular aggregates with short range order at low surface concentrations, and then transition to fibres with long range order at high surface concentrations.

In order to investigate the ability of Beta 9H to form gold nanoparticles, the peptide is deposited on the air–water interface and compressed to different surface pressures after which solutions of $HAuCl_4$ are injected into the subphase using an injection port below the interface. During the experiment, the interface is visualized using a Brewster angle microscope. The Au^{3+} ions are left to incubate in the Langmuir trough for a period of 10 h. Brewster Angle microscopy images of the interface with the peptide at a surface pressure of 30 mN m^{-1} before and after the 10-hour incubation period are shown in Fig. 3. The images show that the Beta 9H peptide forms discrete domains before the addition of gold and that the interface considerably brightens as interfacial gold structures form during the 10-hour incubation period.

Brewster angle microscopy is a measure of changes of indices of refraction at the air–water interface, and the increased brightness indicates that a material of higher refractive index has formed on the interface.[45] In order to probe the nature of these structures found on the interface after the incubation period, samples are taken from the air–water interface using a Langmuir–Schaefer technique onto carbon-coated copper Transmission Electron Microscopy (TEM) grids. The TEM images obtained are shown in Fig. 4 with their corresponding electron diffraction patterns. The images and diffraction patterns in Fig. 4 show samples collected at 30 mN m^{-1}, 40 mN m^{-1}, and 50 mN m^{-1}.

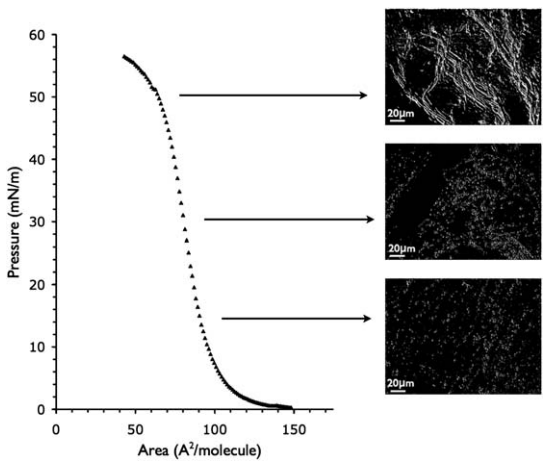

Fig. 2 The surface pressure-area isotherm and Brewster angle microscopy images obtained for Beta 9H at a temperature of 25 °C on a deionized water subphase (pH ~ 5.5).

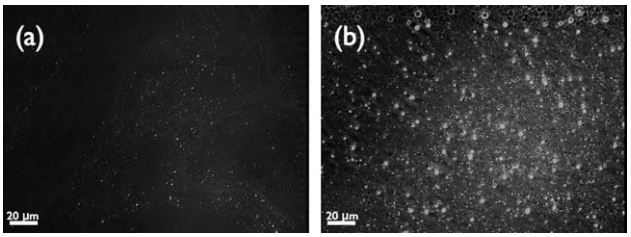

Fig. 3 Brewster angle microscopy images taken at a surface pressure of 30 mN m^{-1} (a) before incubation with Au^{3+} ions (b) after incubation with Au^{3+} ions. The width of the images is 220 μm.

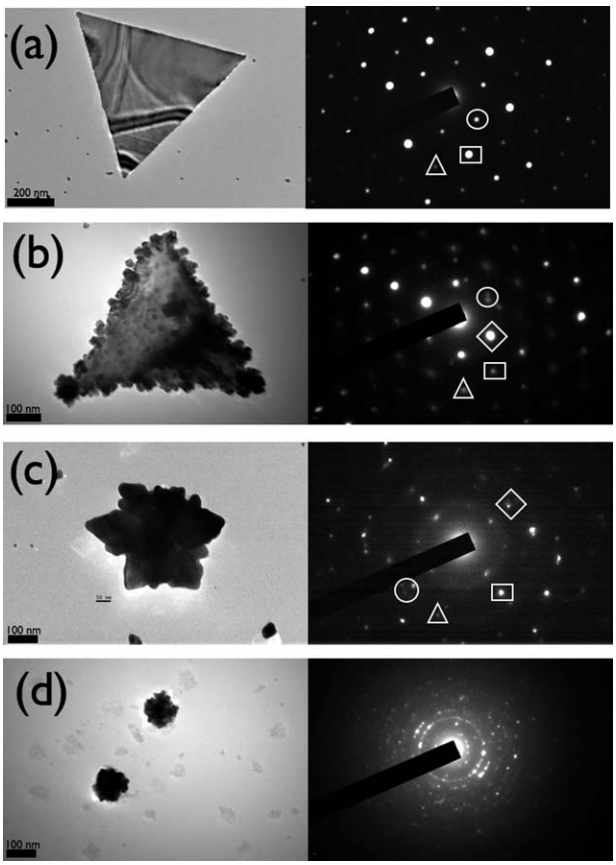

Fig. 4 The TEM images and corresponding electron diffraction patterns at varying surface pressures: (a) Beta 9H collected at a surface pressure of 30mN m^{-1}, circled diffraction spot corresponds to 1/3 {422}; square: {220}; triangle: {311} (b) Beta 9H collected at a surface pressure of 40 mN m^{-1}, circle indicates out of phase diffraction spots; diamond: {111}; square: {220}; triangle:{311} (c) Beta 9H collected at surface pressure of 50 mN m^{-1}, circle indicates multiple out of phase diffraction spots; diamond: {111}; square: {220}; triangle: {311} (d) Beta 3 collected at a surface pressure of 30 mN/m.

The image collected at 30 mN m^{-1} shows an equilateral triangle with sides of approximately 800 nm. The corresponding electron diffraction pattern indicates that the triangle is a single crystal of hexagonal symmetry and can be indexed using the fcc structure of gold, having a lattice constant of $a = 4.07$ Å. The hexagonal pattern arising in the diffraction indicates that {111} facets bound the crystal.[46,47] The strongest peaks obtained are for the peaks pertaining to the {220} reflections as seen in Fig. 4a. Using the fcc crystal structure and the lattice constant, one can calculate the spacing of planes which is 2.348 Å for {111}, 1.441 Å for {220}, and 1.225 Å for {311}.

At 40 mN m^{-1}, Fig. 4 indicates that the triangular crystal formed is rougher and smaller with sides of approximately 510 nm. The diffraction pattern still has hexagonal symmetry similar to that of the triangle formed at 30mN/m. However, the electron diffraction pattern has small differences to that shown for 30 mN m^{-1}. There are often coupled diffraction peaks in the place of a single diffraction spot, suggesting that the rougher triangle is made up of multiple single crystals that are formed out of phase.

At 50 mN m^{-1}, we observe through the TEM image that the structure formed is no longer a triangle, but instead a "star-like" figure that has a diameter from point to point of approximately 460 nm. Qualitatively, at these higher pressures, these "star-like" structures appear to be formed from several overlapping triangles. The electron diffraction pattern of this structure upon close examination still has the hexagonal symmetry found in the other two gold structures. However, the multiple spots effect is more pronounced indicating that the structure is more polycrystalline in nature than the rough triangle.

We have also conducted experiments at surface pressures below 30 mN m^{-1}, ranging from 5 mN m^{-1} to 20 mN m^{-1}. In these experiments, we also observe the formation of triangular structures similar to those formed at 30mN m^{-1} in Fig. 4, but, at surface pressures below 30 mN m^{-1}, the yield of triangles is lower. The average number of triangles and related structures found in sample areas of the TEM grids (approximately 750 μm^2) at various surface pressures are shown in the table in Fig. 5. From the data in this table, we see a significant drop in yield when the surface pressure is below 30 mN m^{-1}. By performing a mass balance, we found that approximately 17.5% of gold ions added to the subphase are found within the resultant triangular platelets at a surface pressure of 30 mN m^{-1}. This number significantly decreases for 20 mN m^{-1}, 10 mN m^{-1}, and 5 mN m^{-1} in which the percentage of gold ions in the triangles are 4.8%, 3.9%, and 4.8% respectively. We attribute the decrease in yield to be due to the lower number of peptide aggregates present between the pressures of 5–20 mN m^{-1}. Sine the total amount of peptide at the interface is constant at all surface pressures, compression only changes the surface concentration. Additionally, we are not losing peptide to the subphase (data shown in ESI,† Fig. 1). Therefore, we hypothesize that an aggregate of a critical size is necessary for the formation of the single crystal triangle. Additional Brewster angle microscopy images showing the relationship between the aggregates formed by peptide molecules and the resultant gold crystals is shown in ESI,† Fig. 2. This phenomena also explains why at higher surface pressures, as is the case for 40 mN m^{-1} and 50 mN m^{-1}, the electron diffraction and TEM images indicate the presence of multiple single crystals

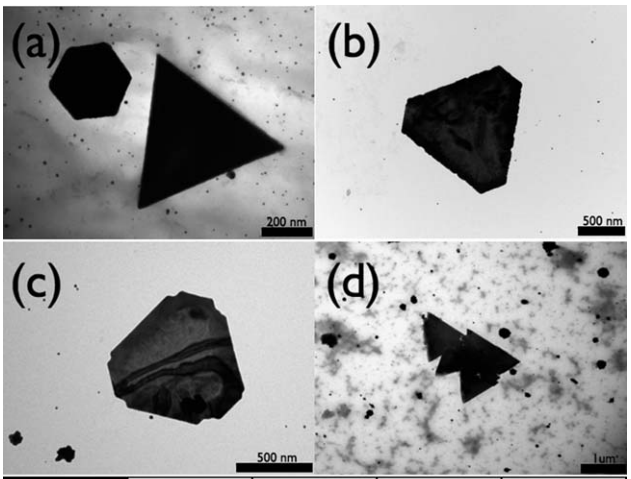

Table	5mN/m	10mN/m	20mN/m	30mN/m
Quantity (triangles or related structures in 742 μm^2 Area)	4.36±3.17	2.50±1.97	6.34±4.58	37.06±21.10
Average Area (μm^2)	0.41±0.37	0.63±0.56	0.34±0.33	0.23±0.04

Fig. 5 TEM images of triangular nanoplatelets and related structures: (a) triangle and hexagon (b) truncated triangle (c) truncated triangle exhibiting further growth (d) saw tooth structure. Table analyzing the average size and number of triangles and related structures at surface pressures between 5–30 mN m^{-1} in sample areas of 742 μ^2.

since the peptide aggregates are much closer together at these higher surface pressures.

The proximity of the peptides changes between 80 $Å^2$/molecule ($\Pi = 30$ mN m^{-1}) and 65 $Å^2$/molecule ($\Pi = 50$ mN m^{-1}) as can be seen in Fig. 2. As the peptide film is compressed the peptides no longer have space to arrange themselves in their preferred orientation at the interface. Similar phenomena has been observed upon compression of calcium carbonate templating molecules in which an increase in surface pressure caused the molecules to tilt[48] in one case exposing a different functional group to the interface.[21] We believe that this change in proximity of neighbouring peptides causes imidazole groups in the histidine residues of the peptides to no longer always be in the plane of the air–water interface leading to multiple single crystals being formed out of phase at the higher surface pressures.

Numerous samples obtained from these experiments also show structures related to triangles such as hexagons, truncated triangles, and saw tooth structures. Images of these structures can be seen in Fig. 5. The hexagons and truncated triangles are found in samples obtained from surface pressures of 30 mN m^{-1} and lower. The size of these structures indicates that the hexagon forms first and, subsequently, growth on three sides of the hexagon are suppressed to form a truncated triangle, and, finally, an equilateral triangle. This mode of growth, called the "silver halide model" has been observed for other fcc gold and silver nanostructures and has been explained by twinning in the [111]

direction, parallel to the {111} facets, that creates convex and concave side crystal facets. The stabilization energy of the convex side is lower than the concave side resulting in a slower growth rate for the convex side. This causes the eventual disappearance of the concave side, leaving a triangular prism.[10] At pressures greater than 30 mN m^{-1}, the saw tooth structure forms and appears to be a series of triangles connected along their vertices. We again hypothesize that this is a result of the proximity of peptide aggregates at higher pressures.

In order to try to understand the formation of these triangular and related structures, two additional experiments are conducted. First, Atomic Force Microscopy (AFM) is applied to determine the thickness of these structures. The AFM measurements are shown in Fig. 6. They indicate that the truncated triangle has a thickness of approximately 20 nm. Therefore, the structures we have been observing are confirmed to platelet structures and not pyramidal. The thinness of these structures is also confirmed using electron diffraction with tilting. In Fig. 4a, the diffraction pattern corresponding to the triangle formed at 30 mN m^{-1} shows the forbidden 1/3 {422} reflection. This reflection is only seen in platelet structures in which the surface of the gold is flat.[29,47,49,50]

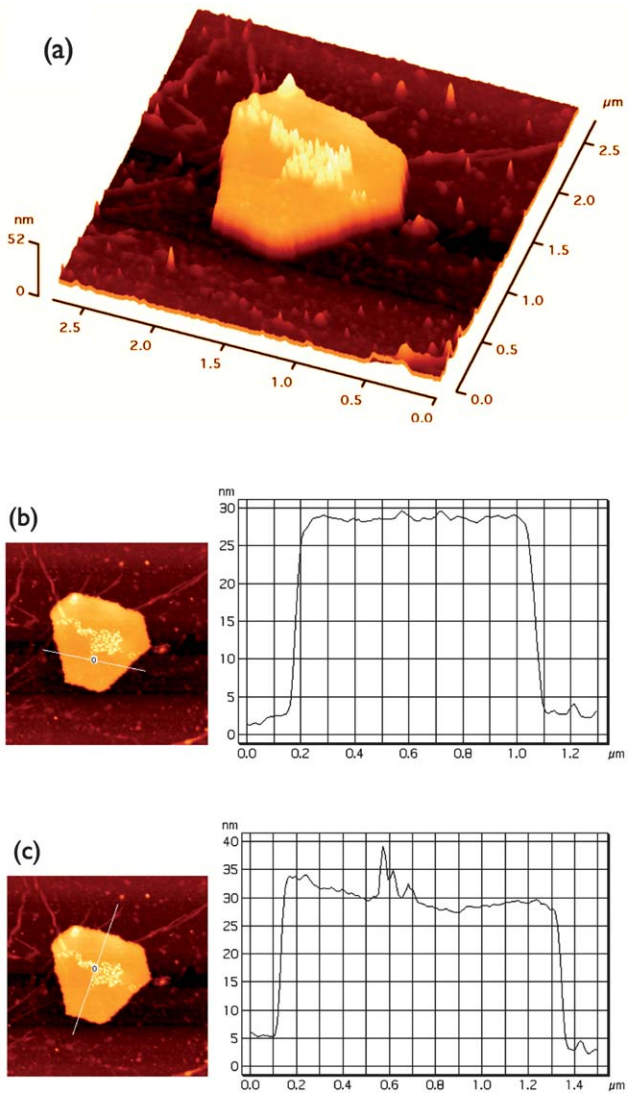

Fig. 6 AFM images obtained for a truncated triangle at a surface pressure of 30mN m^{-1}. (a) Three dimensional image (b) and (c) cross section and corresponding thickness profile.

Second, a control experiment is conducted at 30 mN m^{-1} using the Beta 3 peptide that contains no histidine. The TEM images and diffraction patterns for these experiments are shown in Fig. 4d. Clearly, gold was reduced at the interface. However, the formation of triangular platelets and related structures did not occur. Instead, we observe circular particles with diameters of approximately 100 nm and no preferential growth of any particular plane of gold. This control experiment clearly indicates that the reduction of gold in our system is attributed to the tryptophan residue in both sequences, but that the histidine residue is responsible for providing a directionality of growth and the formation of triangular platelets with the {111} face parallel to the air–water interface. Many metals have facets dominated by the {111} facet, indicating a low energy plane.[44] We suggest that the mechanism of growth of these triangular particles relies on the imidazole side chain binding to the {111} face of gold and thus inhibiting the growth of that particular plane or, in other words, acting as a capping agent. These fast growing facets will eventually disappear during growth, resulting in a crystal dominated by the slow growing facets.[51] This phenomena of imidazole capping the {111} facet has been observed previously in other imidazole containing molecules such as ionic liquids[49] and C18-imidazole surfactants.[52] In the case of the ionic liquid study, higher concentrations produce plate-like particles similar to those observed at our interfaces, while low concentrations produce polyhedron like particles. This indicated that at lower concentrations, the amount of imidazole containing molecules is not sufficient to inhibit growth of other crystal planes.[49]

Conclusion

We have demonstrated that the rationally designed peptide Beta 9H can form atomically smooth single crystal triangular gold nanoplatelets optimally at surface pressure of 30 mN m^{-1} without the use of extra reducing agents or high temperatures. The rational design has incorporated a tryptophan residue that is responsible for the reduction of Au^{3+} to Au^{0} and histidine residues that inhibit the growth of the {111} facet of gold. In addition, we have shown that by increasing the surface pressure of the Beta 9H peptide film, we promote more complex structures as a function of surface pressure, resulting in a mosaic of structures such as rough triangular platelets, saw tooth structures, and "star-like" structures that, in contrast to low surface pressure structures, are polycrystalline.

The characterization of crystallization using rationally designed peptides confined to interfaces has allowed us to access biomimetic pathways that lead to complexity in metallic nanostructure. These biologically inspired materials synthesis processes illustrate the relationship between a dynamic supramolecular template and the final crystalline product. The formation of single crystalline triangular platelets at low surface pressures and polycrystalline multi-faceted structures at higher pressures suggests a mechanism for growth of the crystalline phase that is more complex than direct epitaxy. Each surface

pressure results in a unique set of growth conditions for the final inorganic structure, indicating that the phase behaviour of the peptide and the dynamics of self-assembly play a critical role in determining the final structure of the composite material.

Acknowledgements

RT and LL acknowledge the support from the Air Force Office of Scientific Research (Grant FA9550-08-1-0041) and the National Science Foundation under Grant No. 0967365. LL acknowledges the National Science Foundation under Grant No. 0934206. WS and HM acknowledge the support from the U.S. Department of Energy, Office of Basic Energy Sciences, Division of Materials Sciences and Engineering (under Award No. DE-FG-02-01ER45935) for material synthesis, microscopic analysis, and growth mechanistic study.

References

1 S. Mann, *Nature*, 1993, **365**, 499–505.
2 C. Zaremba, A. Belcher, M. Fritz, Y. Li, S. Mann, P. Hansma, D. Morse, J. Speck and G. Stucky, *Chem. Mater.*, 1996, **8**, 679–690.
3 S. Weiner and H. Wagner, *Annu. Rev. Mater. Sci.*, 1998, **28**, 271–298.
4 E. Bäuerlein, *Angew. Chem., Int. Ed.*, 2003, **42**, 614–641.
5 E. Katz and I. Willner, *Angew. Chem., Int. Ed.*, 2004, **43**, 6042–6108.
6 S. Eustis and M. El-Sayed, *Chem. Soc. Rev.*, 2006, **35**, 209–217.
7 F. Meldrum and H. Cölfen, *Chem. Rev.*, 2008, **108**, 4332–4432.
8 M. Daniel and D. Astruc, *Chem. Rev.*, 2004, **104**, 293–346.
9 C. Johnson, E. Dujardin, S. Davis, C. Murphy and S. Mann, *J. Mater. Chem.*, 2002, **12**, 1765–1770.
10 M. Grzelczak, J. Pérez-Juste, P. Mulvaney and L. Liz-Marzan, *Chem. Soc. Rev.*, 2008, **37**, 1783–1791.
11 Y. Sun and Y. Xia, *Science*, 2002, **298**, 2176.
12 L. Wang, X. Chen, J. Zhan, Y. Chai, C. Yang, L. Xu, W. Zhuang and B. Jing, *J. Phys. Chem. B*, 2005, **109**, 3189–3194.
13 C. Nehl, H. Liao and J. Hafner, *Nano Lett.*, 2006, **6**, 683–688.
14 N. Rosi and C. Mirkin, *Chem. Rev.*, 2005, **105**, 1547–1562.
15 M. Dickerson, K. Sandhage and R. Naik, *Chem. Rev.*, 2008, **108**, 4935–4978.
16 L. Polavarapu and Q. Xu, *Nanotechnology*, 2008, **19**, 075601.
17 C. Chen, P. Zhang and N. Rosi, *J. Am. Chem. Soc.*, 2008, **130**, 13555–13557.
18 M. Tomczak, D. Glawe and L. Drummy, *J. Am. Chem. Soc.*, 2005, **127**, 12577–12582.
19 Y. Yao, W. Dong, S. Zhu, X. Yu and D. Yan, *Langmuir*, 2009, **25**, 13238–13243.
20 M. Reches and E. Gazit, *Science*, 2003, **300**, 625–627.
21 S. Cavalli, D. C. Popescu, E. E. Tellers, M. R. J. Vos, B. P. Pichon, M. Overhand, H. Rapaport, N. A. J. M. Sommerdijk and A. Kros, *Angew. Chem., Int. Ed.*, 2006, **45**, 739–744.
22 R. Djalali, Y. Chen and H. Matsui, *J. Am. Chem. Soc.*, 2003, **125**, 5873–5879.
23 M. Lamm, N. Sharma, K. Rajagopal, F. Beyer, J. Schneider and D. Pochan, *Adv. Mater.*, 2008, **20**, 447–451.
24 N. Sharma, A. Top, K. Kiick and D. Pochan, *Angew. Chem., Int. Ed.*, 2009, **48**, 7078–7082.
25 M. Iosin, P. Baldeck and S. Astilean, *J. Nanopart. Res.*, 2010, **12**, 2843–2849.
26 J. M. Slocik, M. O. Stone and R. R. Naik, *Small*, 2005, **1**, 1048–1052.
27 S. Brown, M. Sarikaya and E. Johnson, *J. Mol. Biol.*, 2000, **299**, 725–735.
28 R. Mitra and P. Das, *J. Phys. Chem. C*, 2008, **112**, 8159–8166.
29 S. Shankar, A. Rai, B. Ankamwar, A. Singh, A. Ahmad and M. Sastry, *Nat. Mater.*, 2004, **3**, 482–488.
30 P. Alivisatos, *Nat. Biotechnol.*, 2003, **22**, 47–52.
31 T. Arai, P. Kumar, C. Rockstuhl, K. Awazu and J. Tominaga, *J. Opt. A: Pure Appl. Opt.*, 2007, **9**, 699–703.
32 J. Riboh, A. Haes, A. McFarland, C. Yonzon and R. Van Duyne, *J. Phys. Chem. B*, 2003, **107**, 1772–1780.
33 M. Rashid, R. Bhattacharjee, A. Kotal and T. Mandal, *Langmuir*, 2006, **22**, 7141–7143.
34 L. Hirsch, R. Stafford, J. Bankson, S. Sershen, B. Rivera, R. Price, J. Hazle, N. Halas and J. West, *Proc. Natl. Acad. Sci. U. S. A.*, 2003, **100**, 13549–13554.
35 S. Shankar, A. Rai, A. Ahmad and M. Sastry, *Chem. Mater.*, 2005, **17**, 566–572.
36 C. Hansen, F. Westerlund, K. Moth-Poulsen, R. Ravindranath, S. Valiyaveettil and T. Bjornholm, *Langmuir*, 2008, **24**, 3905–3910.
37 K. Nørgaard and T. Bjørnholm, *Chem. Commun.*, 2005, 1812–1823.
38 N. Markovich, R. Volinsky and R. Jelinek, *J. Am. Chem. Soc.*, 2009, **131**, 2430–2431.
39 N. Kumar, C. Maldarelli, C. Steiner and A. Couzis, *Langmuir*, 2001, **17**, 7789–7797.
40 P. Chou and G. Fasman, *Biochemistry*, 1974, **13**, 222–245.
41 H. Xiong, B. Buckwalter, H. Shieh and M. Hecht, *Proc. Natl. Acad. Sci. U. S. A.*, 1995, **92**, 6349–6353.
42 B. Glisic, S. Rajkovic, M. Zivkovic and M. Djuran, *Bioorg. Chem.*, 2010, **38**, 144–148.
43 J. Cuadrado, W. Zhang, W. Hang and V. Majidi, *J. Environ. Monit.*, 2000, **2**, 355–359.
44 L. Leon, P. Logrippo and R. Tu, *Biophys. J.*, 2010, **99**, 2888–2895.
45 C. Lheveder, S. Hénon, R. Mercier, G. Tissot, P. Fournet and J. Meunier, *Rev. Sci. Instrum.*, 1998, **69**, 1446–1450.
46 Y. Shao, Y. Jin and S. Dong, *Chem. Commun.*, 2004, 1104–1105.
47 Y. Sun, B. Mayers and Y. Xia, *Nano Lett.*, 2003, **3**, 675–679.
48 E. DiMasi, S. Y. Kwak, B. P. Pichon and N. A. J. M. Sommerdijk, *CrystEngComm*, 2007, **9**, 1192–1204.
49 J. Zhu, Y. Shen, A. Xie, L. Qiu, Q. Zhang and S. Zhang, *J. Phys. Chem. C*, 2007, **111**, 7629–7633.
50 V. Germain, J. Li, D. Ingert, Z. Wang and M. Pileni, *J. Phys. Chem. B*, 2003, **107**, 8717–8720.
51 Y. Yin and A. Alivisatos, *Nature*, 2004, **437**, 664–670.
52 S. Hsu, K. Hsu, M. Leong and I. Lin, *Dalton Trans.*, 2008, 1924–1931.

